香港浸會大學 HONG KONG BAPTIST UNIVERSITY 地理系 DEPARTMENT OF GEOGRAPHY

Potential role of local contributions to record-breaking high-temperature event in Xiamen, China

Fan Wang
Department of Geography
Hong Kong Baptist University
E-mail: fanwang9604@gmail.com

Contents:

- Introduction
- Methods
- Results and Discussions
- Conclusions

Introduction

Introduction

Extreme high-temperature (EHT) events have occurred frequently in recent years, threatening plant growth, public health, and energy.

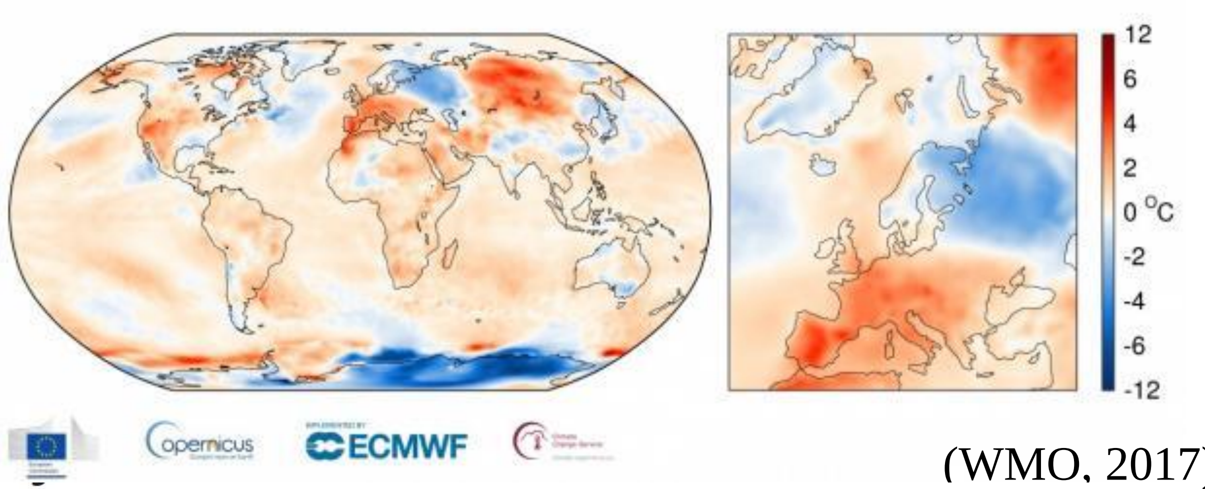

(WMO, 2017)

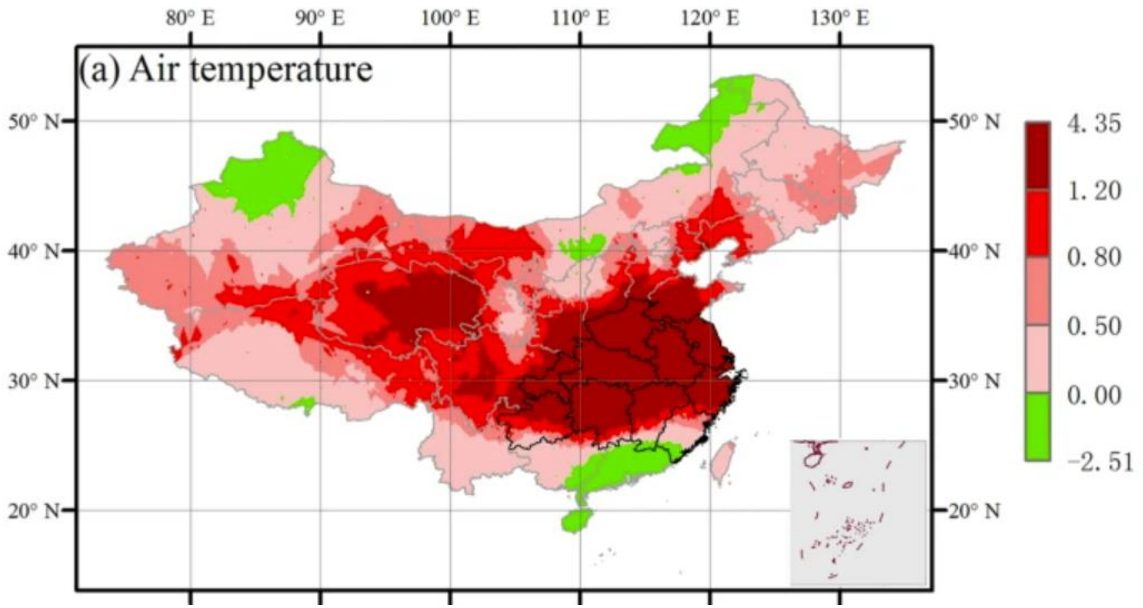

(Yuan et al., 2016)

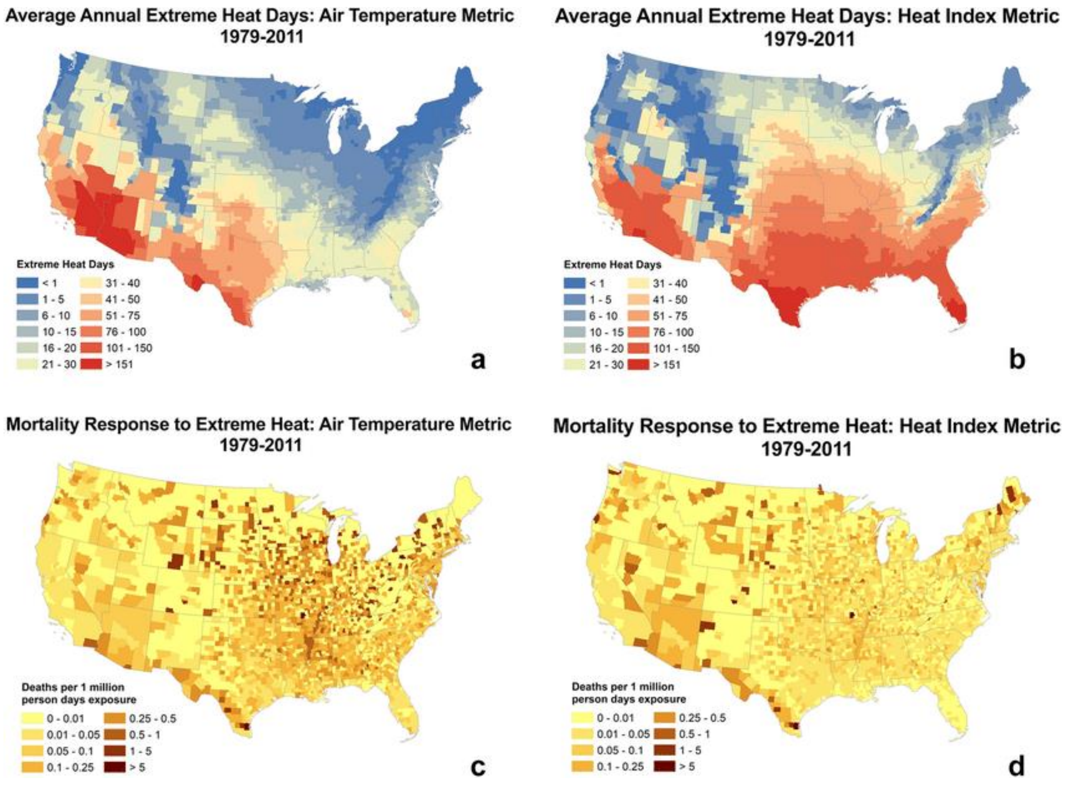

(Jones et al., 2021)

The World Meteorological Organization (WMO, 2013) reported that the number of deaths due to EHT for 2001-2010 increased by 2300% compared to that for 1991-2000.

Three main factors cause the occurrence of EHT events.

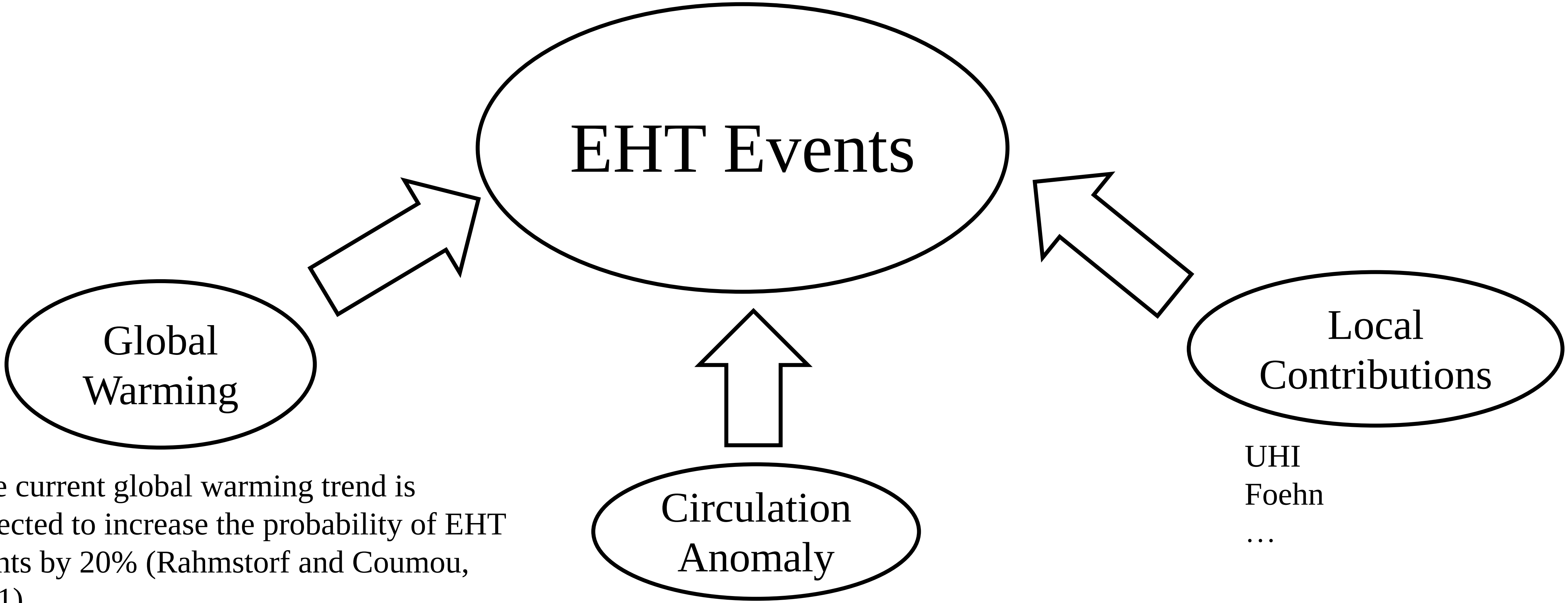

The current global warming trend is expected to increase the probability of EHT events by 20% (Rahmstorf and Coumou, 2011).

- Anomalous anticyclone in Atlantic-Europe.
- Anomalous South Asia high and West Pacific subtropical high in eastern Asia.

UHI
Foehn
…

Introduction

A five-day-lasting heat wave struck Xiamen, China, from 8 to 12 August 2019. The daily maximum temperature reached 39.6 °C in 9 August 2019 and broke the recorded highest daily maximum temperature of 39.2 °C set in 2007.

Source: Climate Bulletin of Fujian Province in 2019

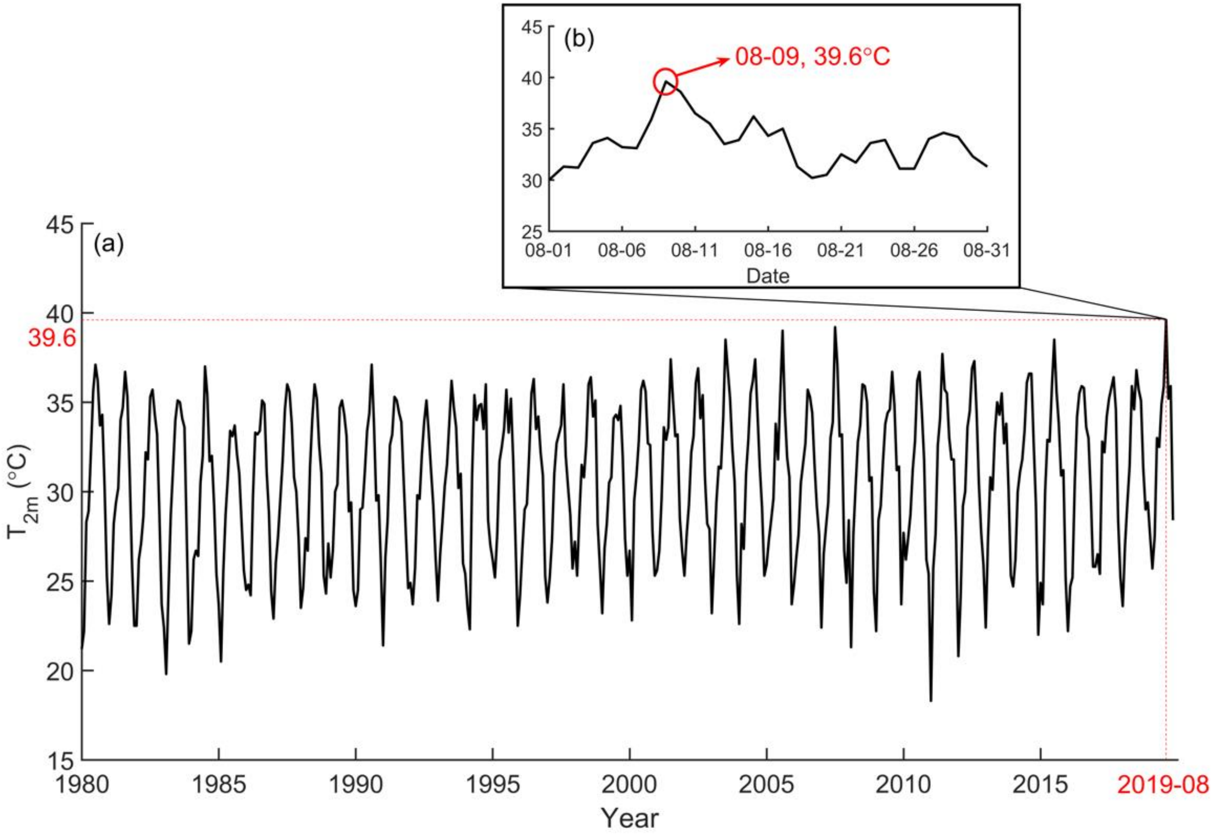

Introduction

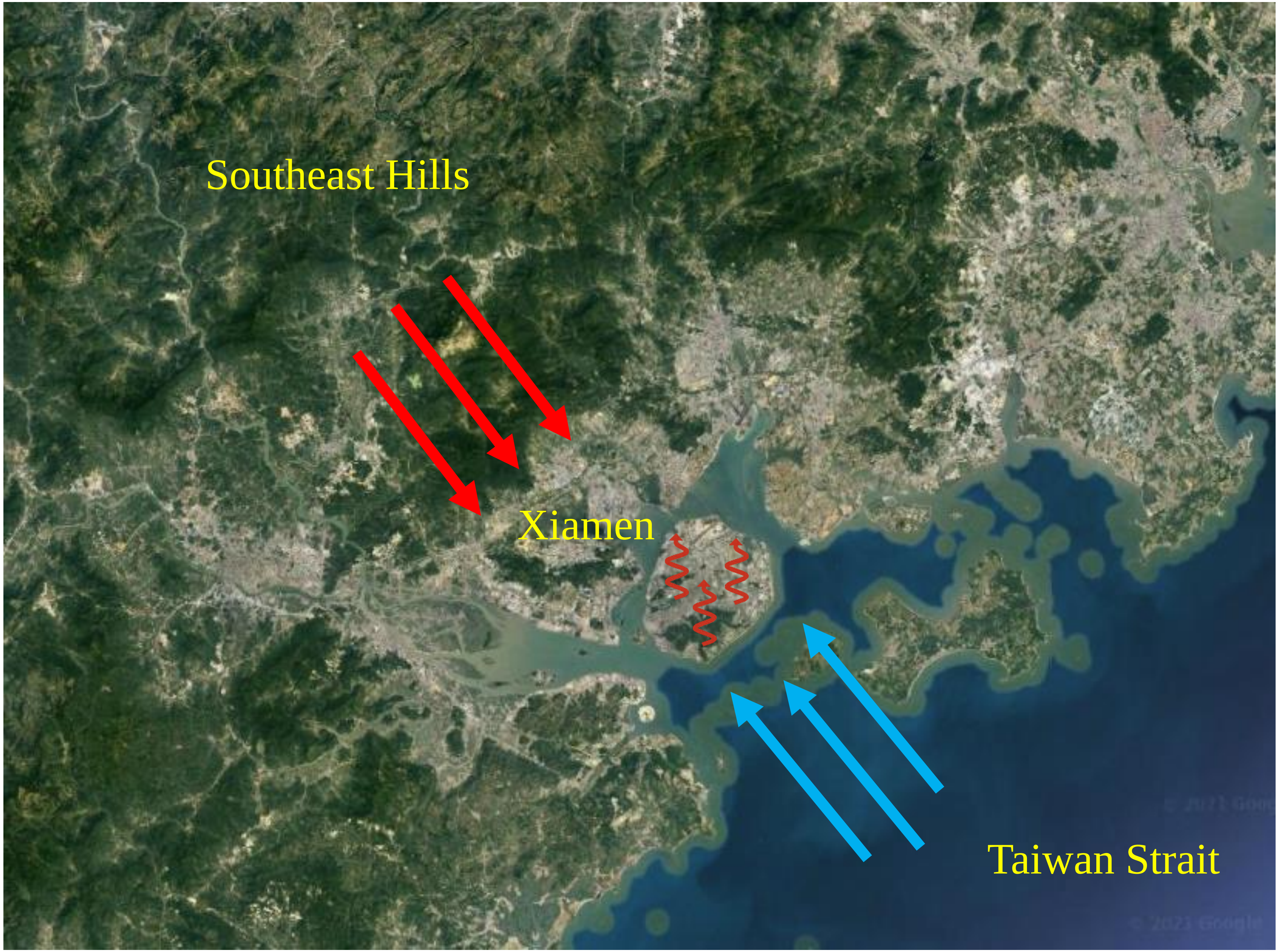

Introduction

In this study, the local contributions to this EHT event were investigated.

We expected to determine the local factors that may have induced this event and to provide theoretical support for improving the prediction of EHT events in the future.

Methods

Methods WRF configurations and data

WRF setup and options of physical schemes.

Domain number	**1**	**2**	**3**	**4**
Coarse domain centre	119°E, 33°N			
Vertical level	36			
Horizontal grid (x, y)	180×200	199×199	202×202	142×151
Horizontal resolution	13.5 km	4.5 km	1.5 km	0.5 km
Microphysics	WSM 5-class (Hong et al., 2004)			
Cumulus scheme	Grell-Freitas (Grell and Freitas, 2014), only used in the first domain			
Land surface scheme	Noah (Tewari et al., 2004)			
Surface layer scheme	MM5 (Jiménez et al., 2012)			
Planetary boundary layer scheme	BouLac (Bougeault and Lacarrere, 1989)			
Long-wave radiation scheme	RRTM (Mlawer et al., 1997)			
Short-wave radiation scheme	Dudhia (Dudhia, 1989)			
Urban surface scheme	BEP-BEM (Martilli et al., 2002; Salamanca and Martilli, 2010)			

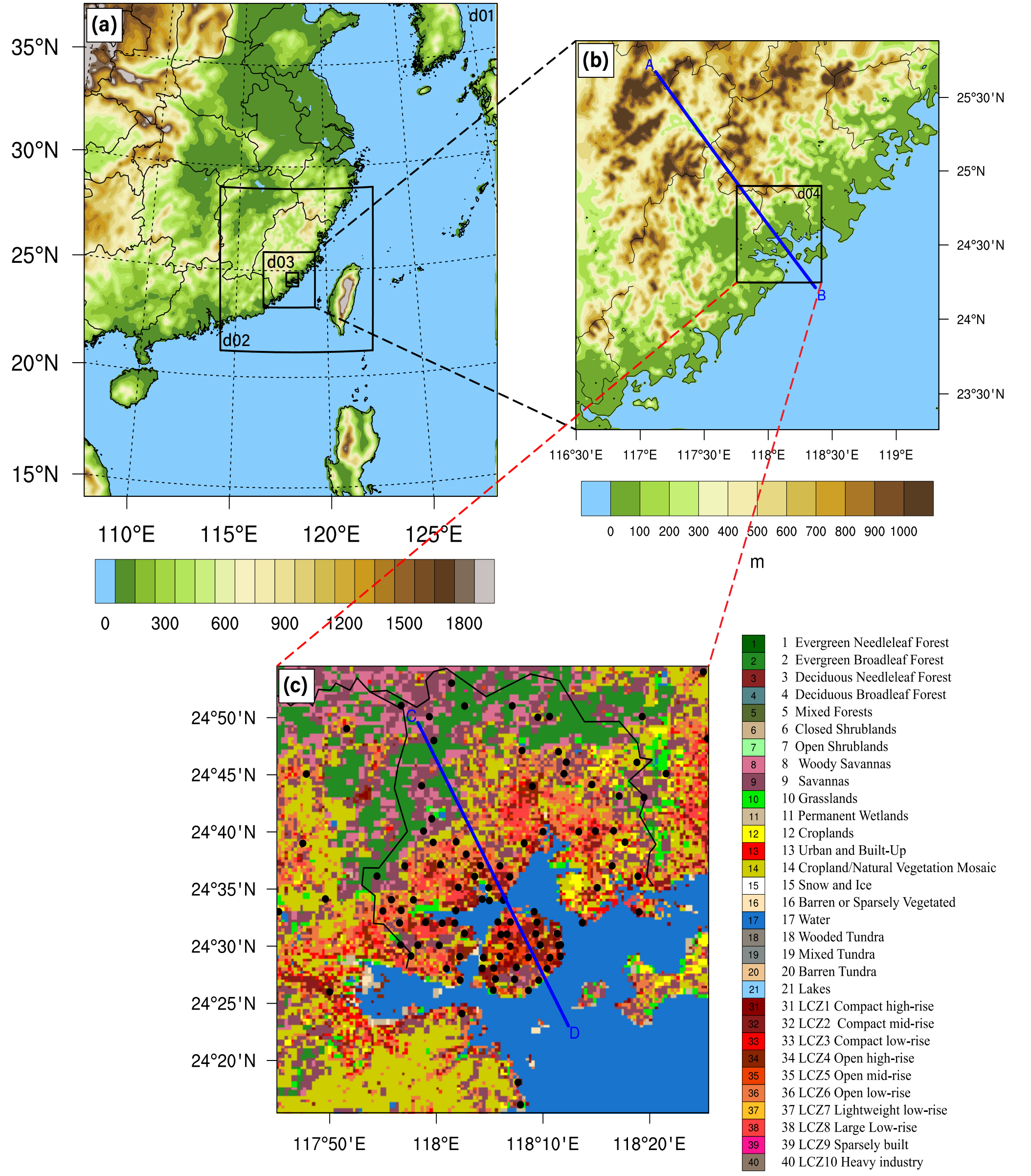

Figure 2. a) WRF simulation area configuration, b) terrain height of the third domain, and c) land-use categories of the innermost domain.

Methods WRF configurations and data

Control case (CTRL)： 2019.8.7-2019.8.10

No-Urban case (NU)： 2019.8.7-2019.8.10 urban land use -> cropland

Sea-Breeze-Day case (SBD)： 2019.8.25-2019.8.28

The initial and boundary conditions: 6-hourly National Centres of Environmental Prediction Final Analysis data set, with a 0.25°×0.25° resolution.

Data for model evaluation: 2m air temperature, 2m relative humidity, and 10m wind speed observed at 91 meteorological stations located in the innermost domain.

Using only the default datasets in the WRF model—such as United States Geological Survey (USGS) and Moderate Resolution Imaging Spectroradiometer datasets (MODIS), which cannot sufficiently subdivide the underlying surface types of cities—may result in deviations in the simulation of urban regional meteorological variables, especially the urban thermal environment and wind field.

Methods WRF/BEP/BEM coupled with LCZ-refined underlying surface data

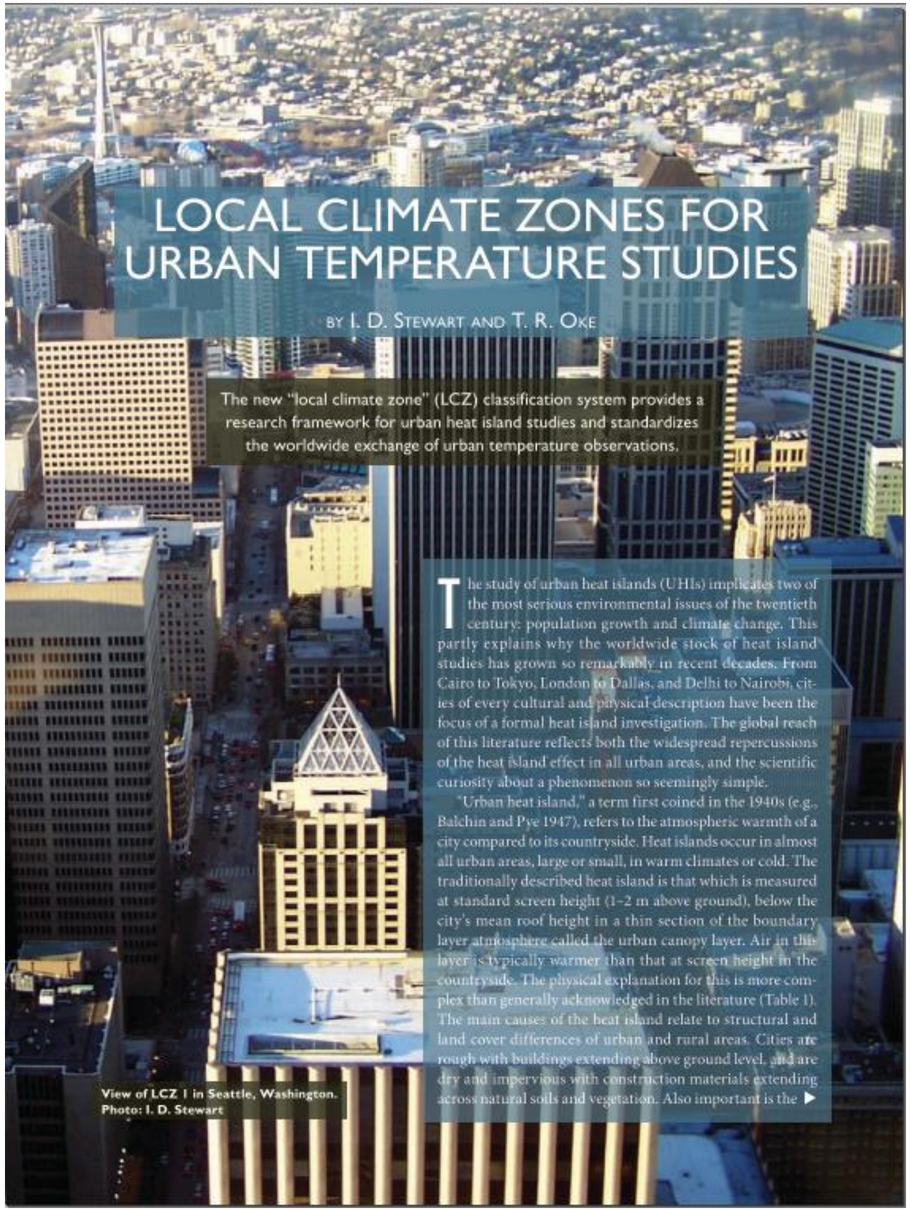
LOCAL CLIMATE ZONES FOR URBAN TEMPERATURE STUDIES

BY I. D. STEWART AND T. R. OKE

The new "local climate zone" (LCZ) classification system provides a research framework for urban heat island studies and standardizes the worldwide exchange of urban temperature observations.

The study of urban heat islands (UHIs) implicates two of the most serious environmental issues of the twentieth century: population growth and climate change. This partly explains why the worldwide stock of heat island studies has grown so remarkably in recent decades. From Cairo to Tokyo, London to Dallas, and Delhi to Nairobi, cities of every cultural and physical description have been the focus of a formal heat island investigation. The global reach of this literature reflects both the widespread repercussions of the heat island effect in all urban areas, and the scientific curiosity about a phenomenon so seemingly simple.

"Urban heat island," a term first coined in the 1940s (e.g., Balchin and Pye 1947), refers to the atmospheric warmth of a city compared to its countryside. Heat islands occur in almost all urban areas, large or small, in warm climates or cold. The traditionally described heat island is that which is measured at standard screen height (1–2 m above ground), below the city's mean roof height in a thin section of the boundary layer atmosphere called the urban canopy layer. Air in this layer is typically warmer than that at screen height in the countryside. The physical explanation for this is more complex than generally acknowledged in the literature (Table 1). The main causes of the heat island relate to structural and land cover differences of urban and rural areas. Cities are rough with buildings extending above ground level, and are dry and impervious with construction materials extending across natural soils and vegetation. Also important is the ▶

View of LCZ 1 in Seattle, Washington. Photo: I. D. Stewart

Local climate zone (LCZ)	Aspect ratio[a]	Sky view factor[b]	Building surface fraction[c]	Impervious surface fraction[d]	Height of roughness elements[e]	Anthropogenic heat flux density[f]
LCZ1 Compact high-rise	>2	0.2–0.4	40–60	40–60	>25	50–300
LCZ2 Compact mid-rise	0.75–1.5	0.3–0.6	40–70	30–50	8–20	<75
LCZ3 Compact low-rise	0.75–1.5	0.2–0.6	40–70	20–40	3–8	<75
LCZ4 Open high-rise	0.75–1.25	0.5–0.7	20–40	30–40	>25	<50
LCZ5 Open mid-rise	0.3–0.75	0.5–0.8	20–40	30–50	8–20	<25
LCZ6 Open low-rise	0.3–0.75	0.6–0.9	20–40	20–40	3–8	<25
LCZ7 Lightweight low-rise	1–2	0.2– 0.5	60–90	<10	2–4	<35
LCZ8 Large low-rise	0.1–0.3	>0.7	30–50	40–50	3–10	<50
LCZ9 Sparsely built	0.1–0.25	>0.8	10–20	<20	3–8	<10
LCZ10 Heavy industry	0.2–0.5	0.6–0.9	20–30	20–40	5–15	>300
LCZA Dense trees	>1	<0.4	<10	<10	3–30	0
LCZB Scattered trees	0.25–0.75	0.5–0.8	<10	<10	3–15	0
LCZC Bush, scrub	0.25–1.0	>0.9	<10	<10	<2	0
LCZD Low plants	<0.1	>0.9	<10	<10	<1	0
LCZE Bare rock or paved	<0.1	>0.9	<10	>90	<0.25	0
LCZF Bare soil or sand	<0.1	>0.9	<10	<10	<0.25	0
LCZG Water	<0.1	>0.9	<10	<10	—	0

Stewart, I.D., Oke, T.R., 2012. Local climate zones for urban temperature studies. Bull. Am. Meteorol. Soc. 93, 1879–1900. https://doi.org/10.1175/BAMS-D-11-00019.1.

基于WU

LCZ分类结果

制作基本

（1）运用

下载

在SA

（2）创建

该步

外，

混乱

（3）生成

运用

分辨

分类

（4）建立

LCZ

据。为后期

练样本较少

态机理相对

gle Earth 高

，直到LCZ

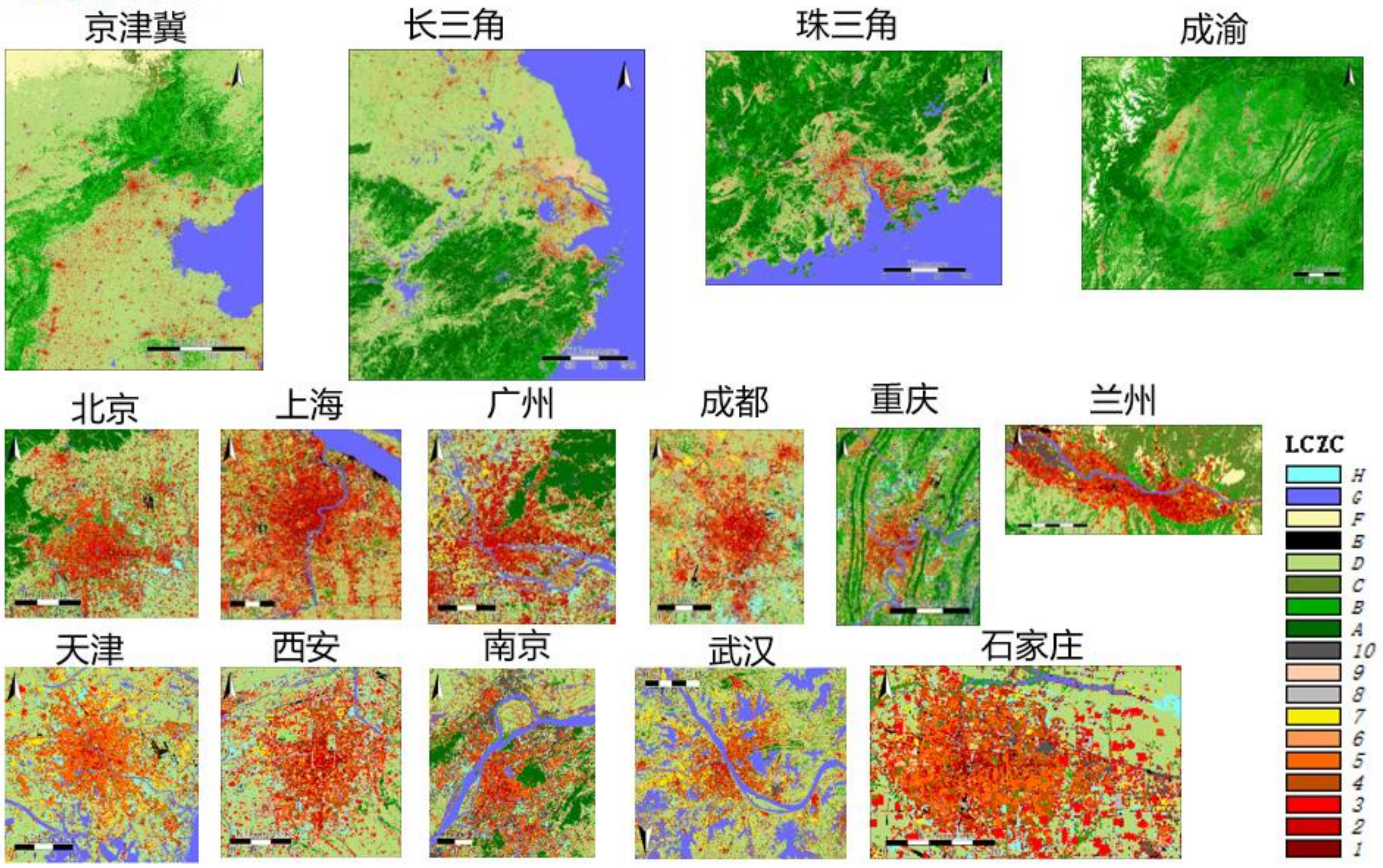

中国四大城市群及部分大城市的LCZ 分类结果

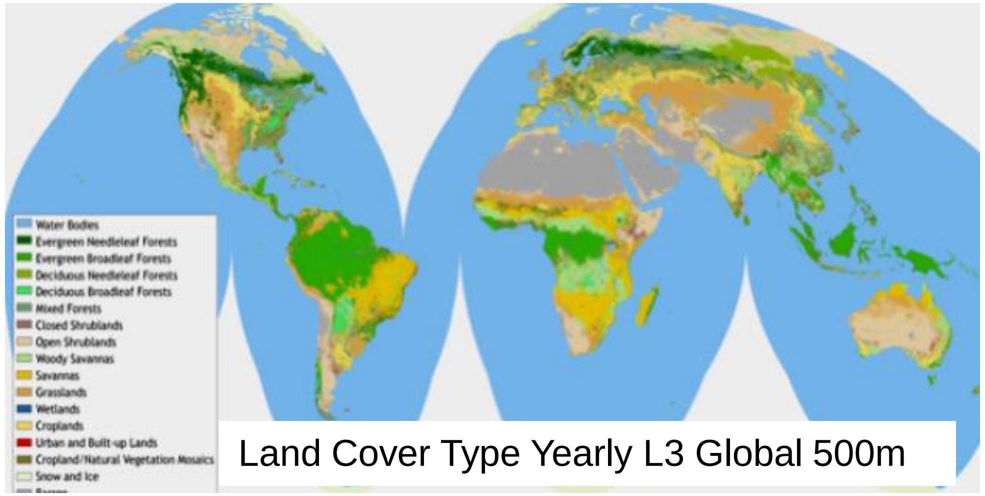

MODIS

geo_em_d0*

WRF

URBPARM.TBL

LCZ map

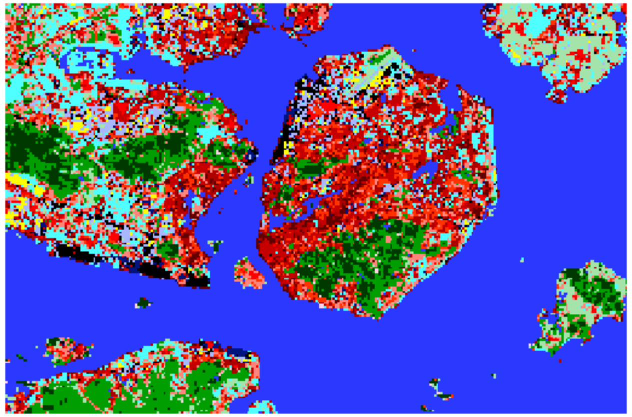

Simplified table of surface property values for local climate zones (Source: Stewart and Oke, 2012).

Local climate zone (LCZ)	Aspect ratio[a]	Sky view factor[b]	Building surface fraction[c]	Impervious surface fraction[d]	Height of roughness elements[e]	Anthropogenic heat flux density[f]
LCZ1 Compact high-rise	>2	0.2–0.4	40–60	40–60	>25	50–300
LCZ2 Compact mid-rise	0.75–1.5	0.3–0.6	40–70	30–50	8–20	<75
LCZ3 Compact low-rise	0.75–1.5	0.2–0.6	40–70	20–40	3–8	<75
LCZ4 Open high-rise	0.75–1.25	0.5–0.7	20–40	30–40	>25	<50
LCZ5 Open mid-rise	0.3–0.75	0.5–0.8	20–40	30–50	8–20	<25
LCZ6 Open low-rise	0.3–0.75	0.6–0.9	20–40	20–40	3–8	<25
LCZ7 Lightweight low-rise	1–2	0.2– 0.5	60–90	<10	2–4	<35
LCZ8 Large low-rise	0.1–0.3	>0.7	30–50	40–50	3–10	<50
LCZ9 Sparsely built	0.1–0.25	>0.8	10–20	<20	3–8	<10
LCZ10 Heavy industry	0.2–0.5	0.6–0.9	20–30	20–40	5–15	>300

Urban morphological parameters.

Category	Urban fraction	Street width (m) (0°/90° from N)	Building width (m) (0°/90° from N)	5 m	10 m	15 m	20 m	25 m	30 m	50 m	70 m	90 m	110 m
LCZ1	0.95	15/15	33/33						27%	46%	13%	13%	1%
LCZ2	0.95	13/13	22/22		30%	22%	37%	8%	3%				
LCZ3	0.9	6/6	18/18	72%	28%								
LCZ4	0.65	38/38	19/39						27%	46%	13%	13%	1%
LCZ5	0.7	33/33	15/35		30%	22%	37%	8%	3%				
LCZ6	0.65	15/15	12/24	72%	28%								
LCZ7	0.85	20/20	20/40	84%	16%								
LCZ8	0.85	30/30	25/25	66%	34%								
LCZ9	0.3	10/10	18/18	100%									
LCZ10	0.55	25/25	11/33	73%	23%	4%							

Results and Discussions

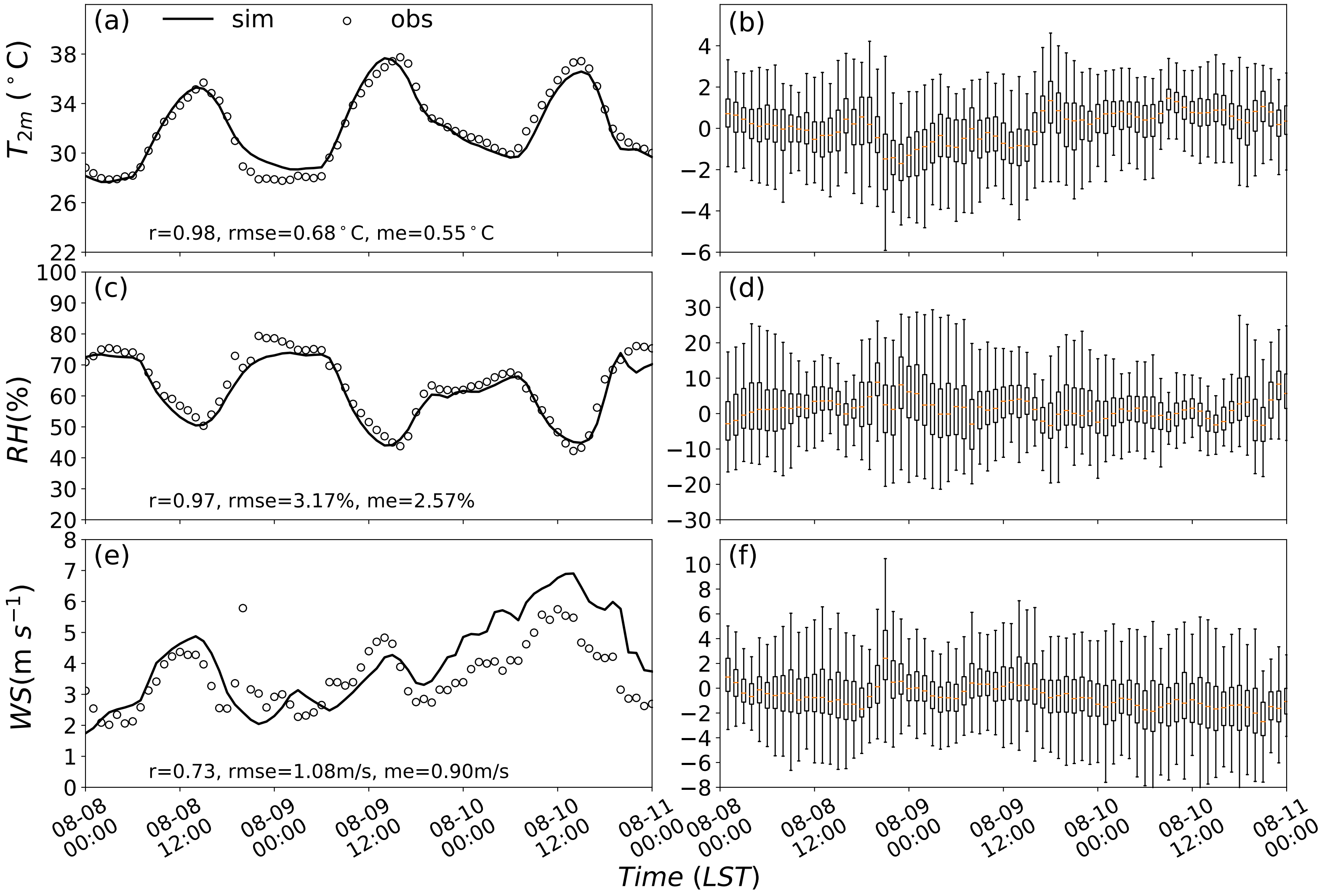

Variation of average observed and simulated a) temperature, c) RH, and e) wind speed, and box plot of differences between them (b, d, f) in each site.

The T_2 deviation at most sites is within ±2 °C, the simulation error of RH is within ± 10%, and the wind speed simulation error is within ± 2 m s^{-1}, all of which are reasonable.

The simulation results successfully reproduced the temporal and spatial distribution characteristics of various meteorological variables during this EHT event.

Results and discussions Synoptic description of the EHT event on 9th August 2019

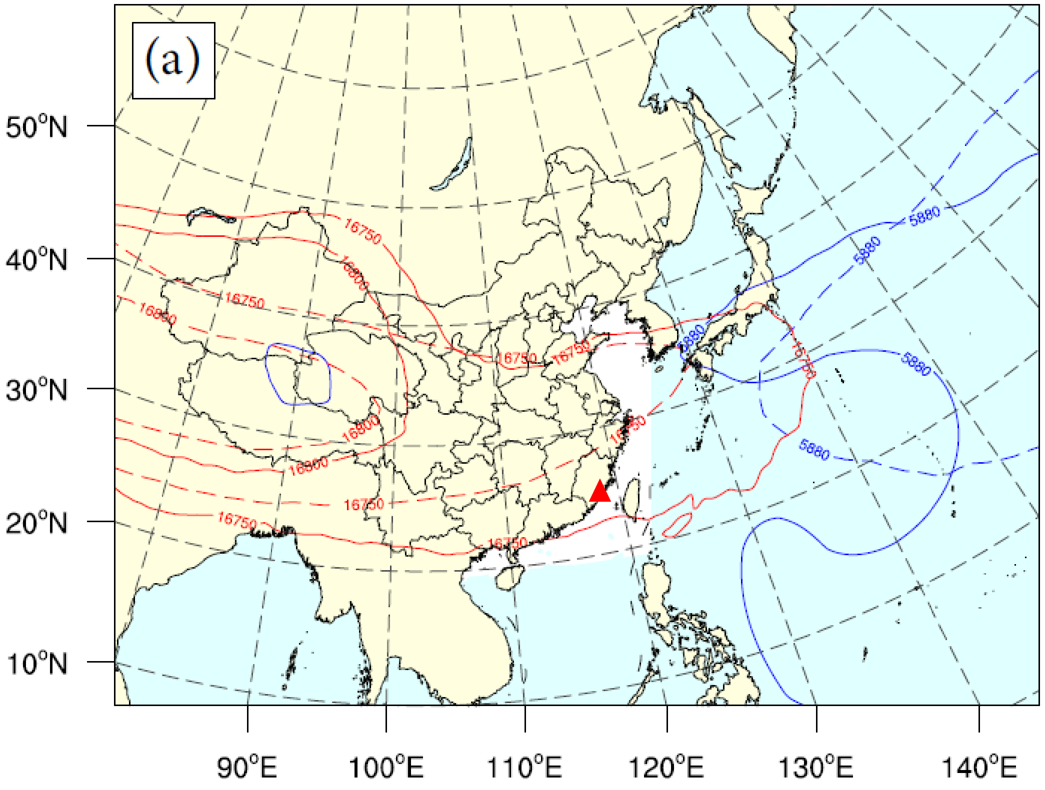

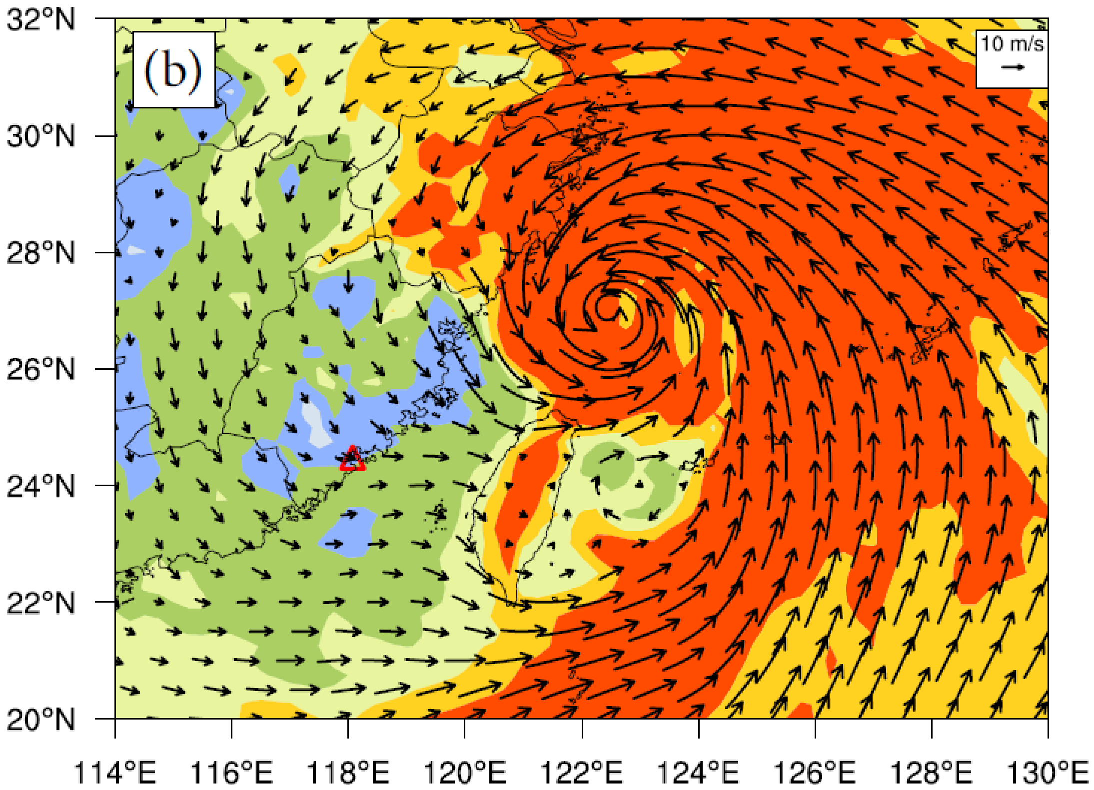

a) South Asia high (red solid lines, unit: dagpm) on 100 hPa and West Pacific subtropical high (blue solid lines, unit: dagpm) on 500 hPa; b) wind field and RH on 925 hPa at 8:00 LST on August 9th, 2019. The red and blue dashed lines are the corresponding climatic characteristic lines. (Red triangle represents the location of Xiamen.)

The SAH body (16760-dagpm line) stretched more eastward.
The WPSH (5880-dagpm line) was more north-westward.

Xiamen area was located on the southwest side of the typhoon centre.
The prevailing wind direction was northwest, and the RH quickly decreased to approximately 60%.

Results and discussions City-warming effect

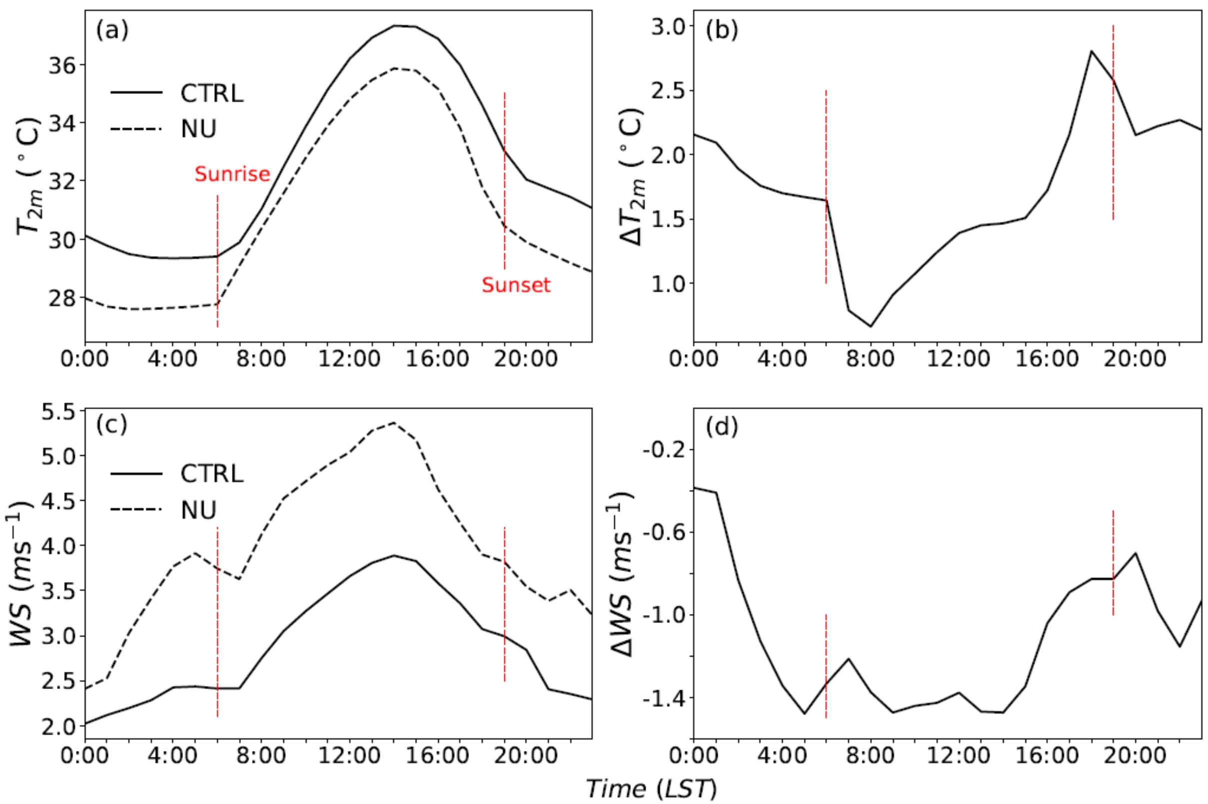

Variation a) of simulated 2-m temperature, b) differences in -m temperature, c) wind speed, and d) difference of wind speed of CTRL and NU on August 9th, 2019.

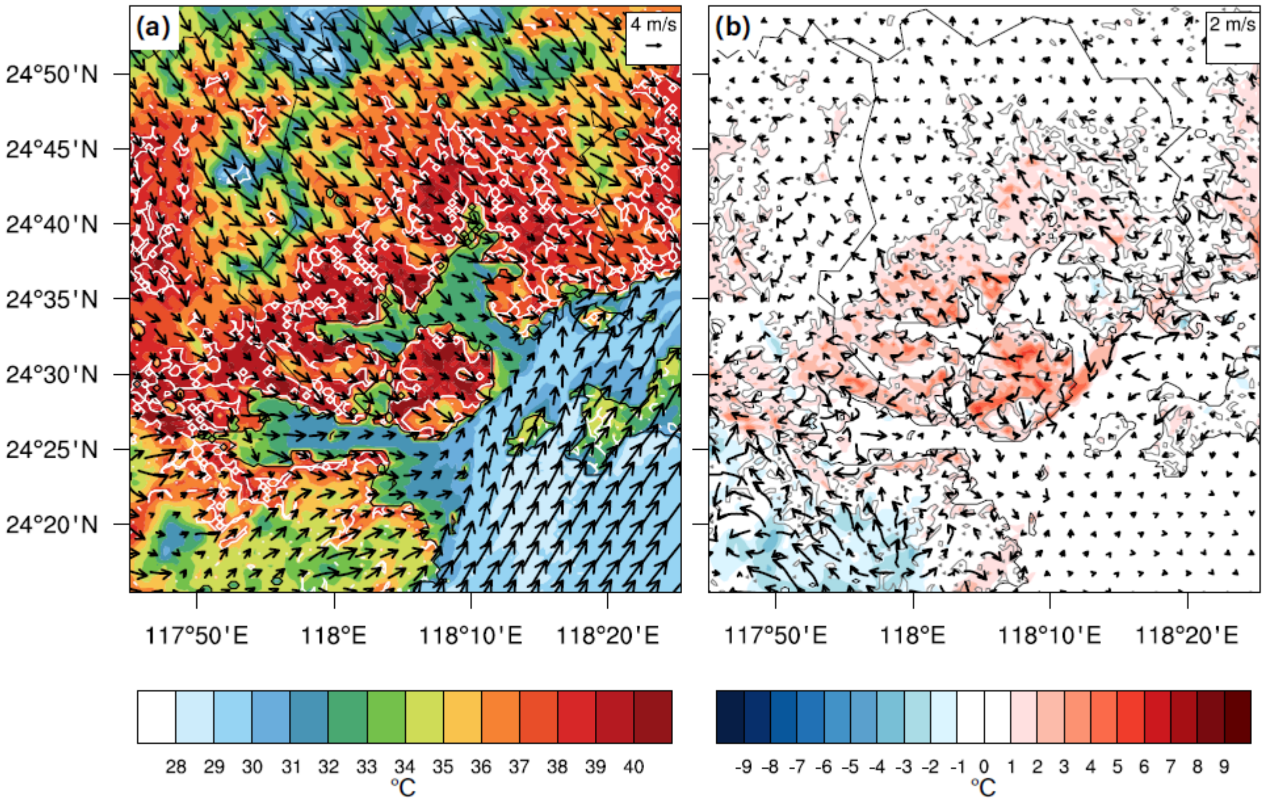

Simulated T2 and WS10 a) in CTRL and b) difference between CTRL and NU (CTRL minus NU) at 15:00 LST on August 9th, 2019.

Cities have a significant warming effect on T2.

The weakening of the wind field by urban buildings hinders the cooling effect of wind on the urban temperature.

Results and discussions Foehn wind warming effect

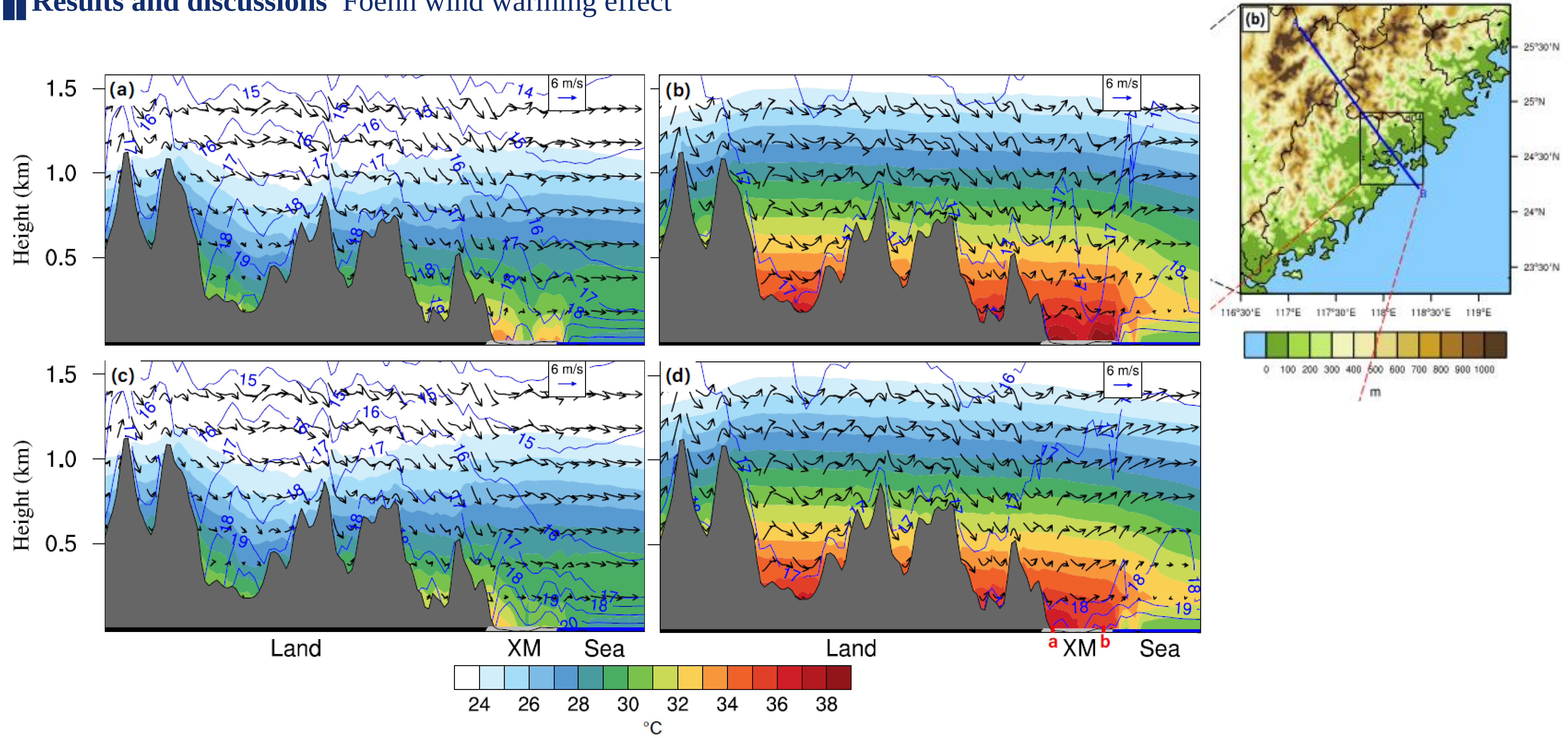

Figure 6. Simulated temperature, water vapor specific humidity, and wind field in the section ('AB' line in Fig. 2(b)) at a) 9:00 LST and b) 15:00 LST in CTRL, and at c) 9:00 LST and d) 15:00 LST in NU on August 9th, 2019.

Results and discussions Foehn wind warming effect

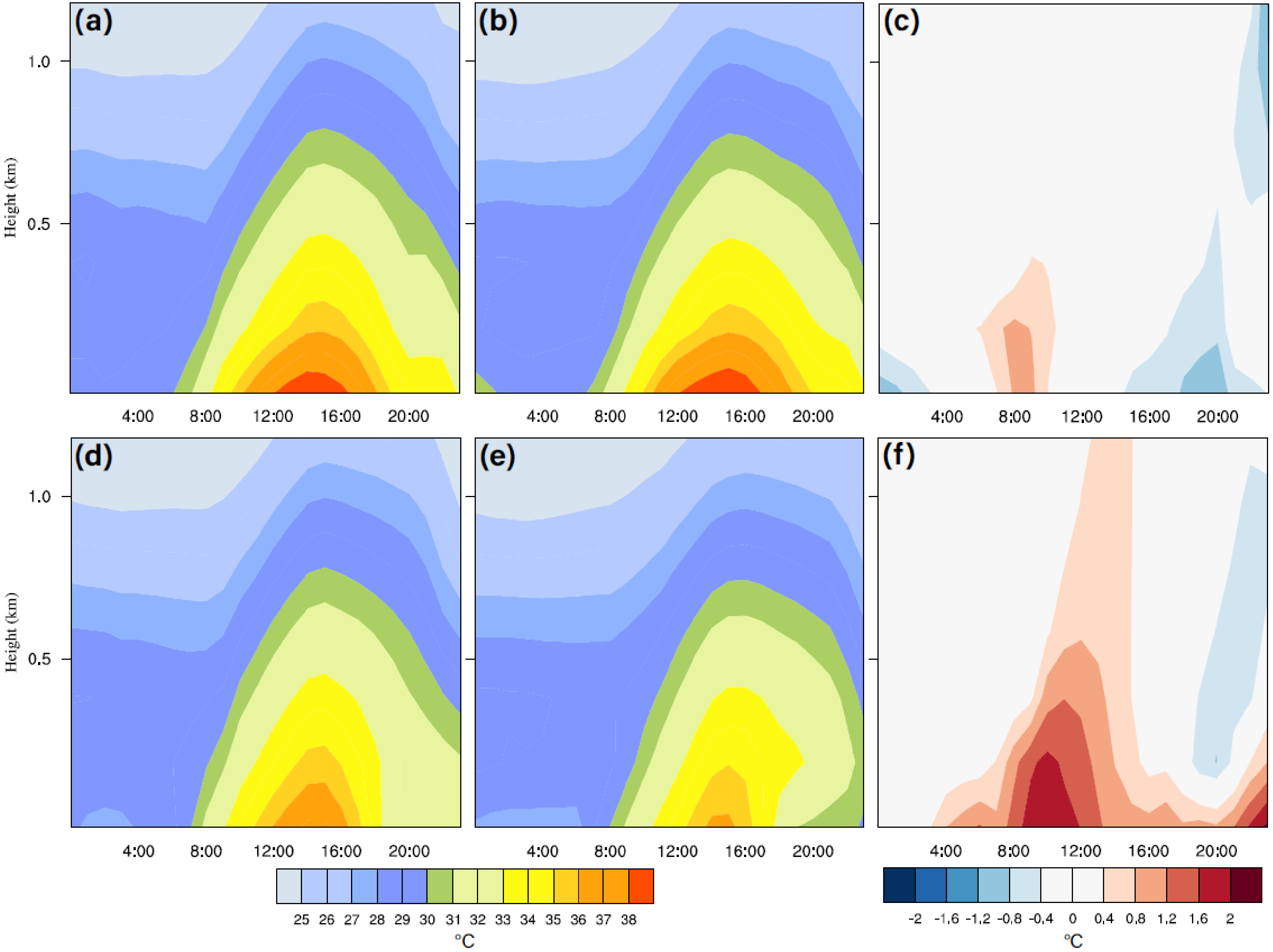

Figure 7. Variation of simulated vertical temperature on a) point ‘a’, b) point ‘b’, and c) difference between them in CTRL; d) point ‘a’, e) point ‘b’, and f) differences between them in NU on August 9th, 2019.

The temperature at point ‘a’ was always higher than that at point ‘b’, undergoing a maximum increase of 1.6–2 °C during 8:00–12:00 LST.

In general, foehn wind directly causes an increase of approximately 2 °C in urban areas close to the hill. Under the influence of background wind, the heat transported to the city gradually spreads to the downstream cities.

Results and discussions Absence of sea breeze cooling effect

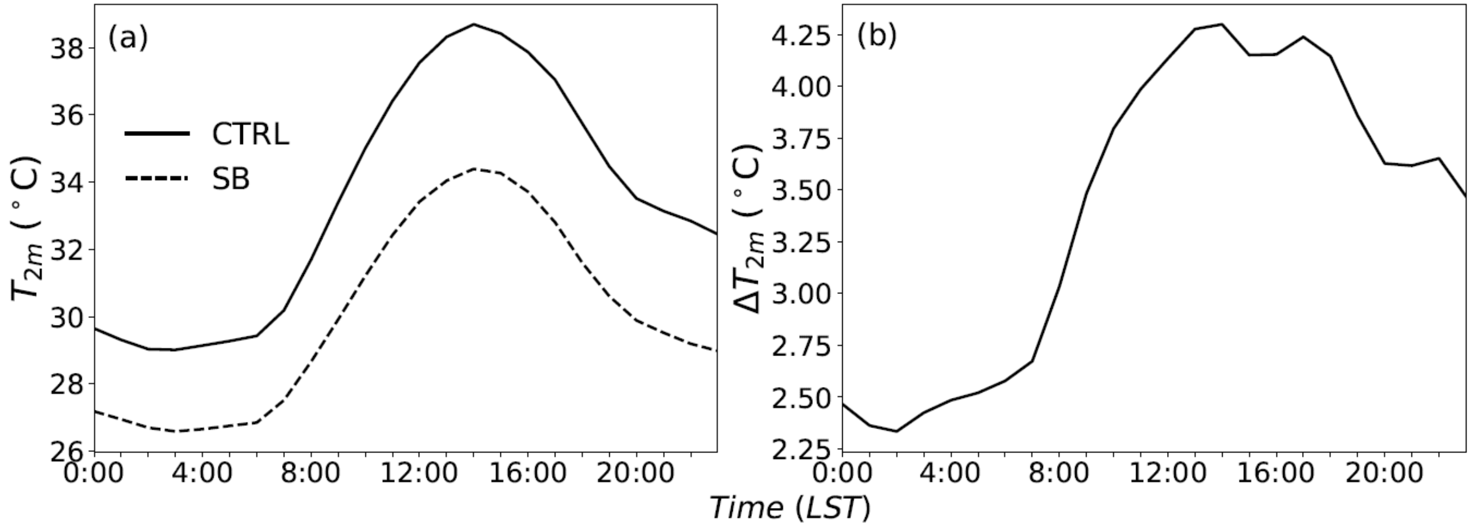

Variation of simulated a) 2-m temperature and b) differences in 2-m temperature on August 9th (CTRL) and 27th (SBD), 2019.

The SBD temperature in urban areas was lower than that on days without a sea breeze, with a difference of 2.3–4.3 °C.

The diurnal temperature difference in urban areas was 9.7 °C without sea breeze; on days with sea breeze, it was only 7.8 °C.

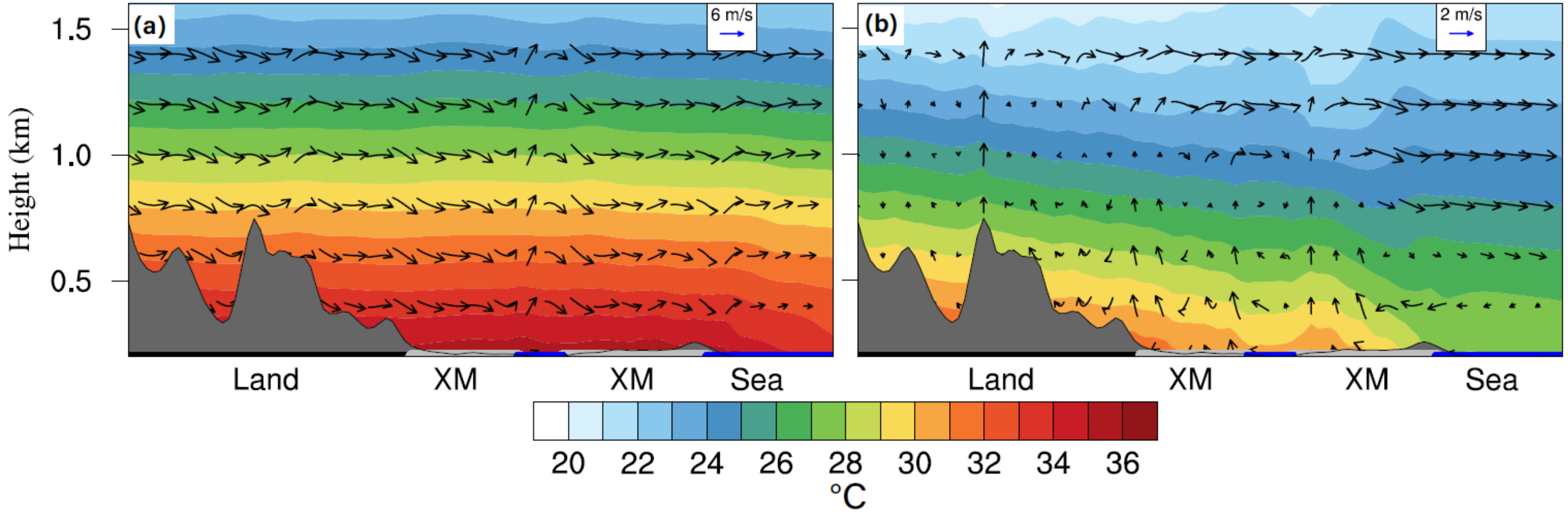

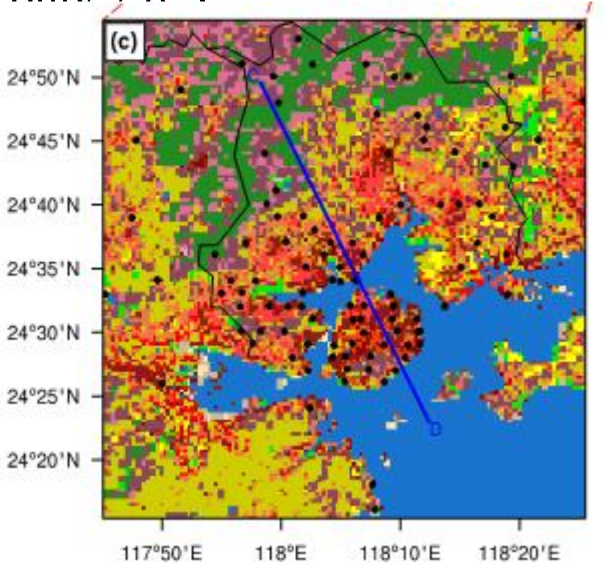

Simulated temperature and wind field in the section ('CD' line in Fig. 2(b)) at 15:00 (LST) on a) August 9th (CTRL) and b) August 27th (SBD), 2019.

Results and discussions Heat budget analysis of the city

$$\text{NET} = \int_{t0}^{t1} \frac{1}{M} \int_{V} \rho \partial_t \mu_d \theta dV dt \ \ (1)$$

$$\text{CONV} = \int_{t0}^{t1} \frac{1}{M} \int_{V} (\nabla \cdot \mathrm{V} \rho \theta) dV dt \ \ (2)$$

$$\text{DIFF} = \text{NET} - \text{CONV} \ (3)$$

Here, *M* is the total mass of air in the control volume, ρ is the density of dry air (kg m^{-3}), and θ is the potential temperature (K). Θ is the coupled potential temperature $\mu_d\theta$ (K), where μ_d is the dry hydrostatic pressure difference between the surface and top of the model (Skamarock et al., 2008).

Results and discussions Heat budget analysis of the city

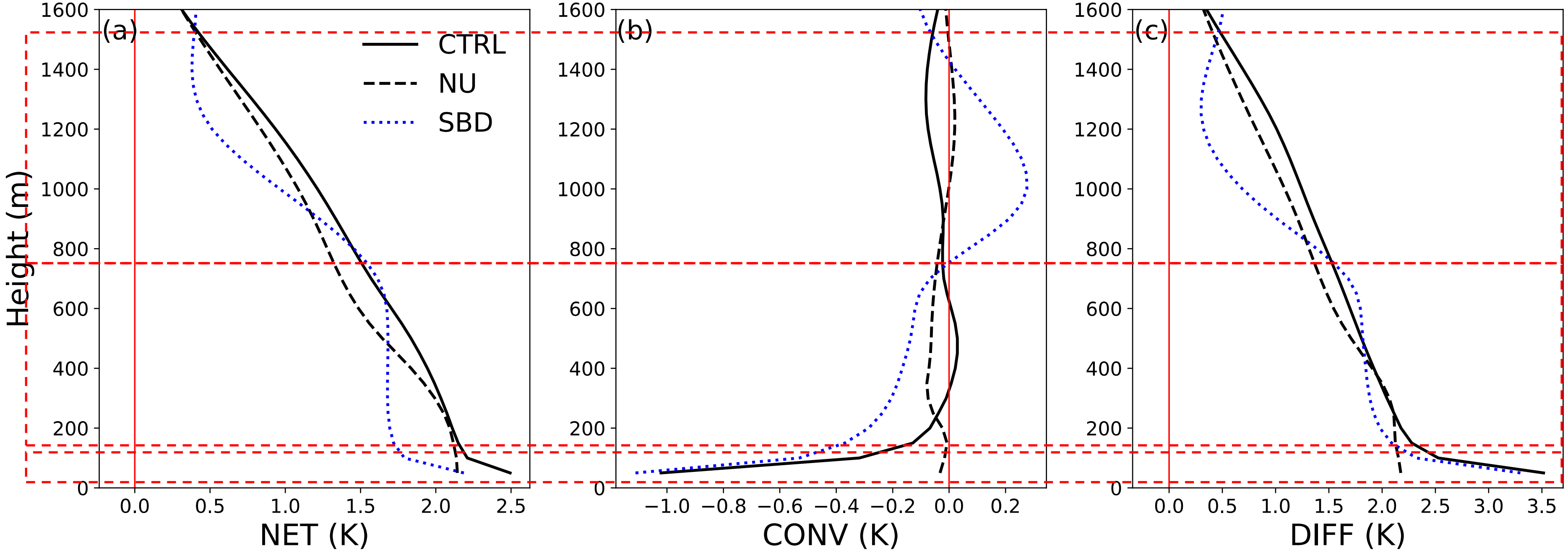

Profiles of urban area average heat budget a) NET, b) CONV, and c) DIFF.

- When the sea breezes occur, the overall heat of the urban canopy is reduced through cold and humid convection, the uplift at the sea breeze front, and the turbulent diffusion of the TIBL.
- The strong northwest wind not only hinders the cooling effects of the sea breeze but also amplifies the influence of the foehn wind; thus, the convective motion increases the heat in the urban area even further.

Results and discussions Wind field characteristics of historical hot days in Xiamen

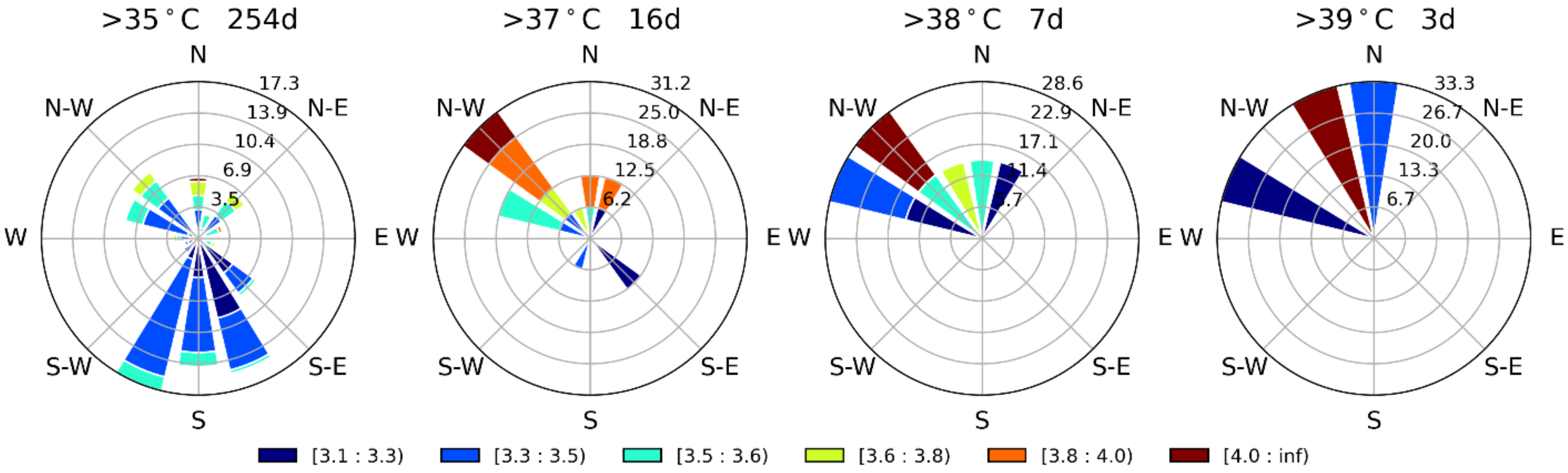

Wind roses of historical (1980-2019) high-temperature days.

Warm airflow from the south is the leading cause of high temperatures in Xiamen.

The occurrence of EHT events is triggered by a combination of the foehn winds caused by the northwest wind and the advancement of the sea breeze being hindered.

Conclusions

Conclusions

- Urbanisation has caused an increase in building height and density, leading to an overall temperature increase of 2–3 °C in the Xiamen area. Tall buildings weaken the cooling effects of convective motions; thus, the UHI intensity can still reach 2.8 °C under strong background winds.

- The foehn winds due to the northwest wind caused the urban area close to the mountain to heat up by about 2 °C; the input heat gradually spread to the downstream city, causing the entire city to heat up.

- The northwest wind also prevented the south-easterly sea breeze from delivering a cold and humid air mass, thus maintaining the high temperature in urban areas; otherwise, the sea breeze may have reduced the urban temperature by 2.3–4.3 °C.

Conclusions

Under the control of the weather system that is conducive to the occurrence of high temperature events, such background wind characteristics and the surface wind weakening by urban buildings are key reasons for this EHT event. In addition, historical EHT events also show similar wind field distributions. The results obtained are informative for predicting future EHT events in Xiamen, although this research is a case study. Xiamen is located in the South Subtropical Monsoon Climate zone, where southeast winds prevail in summer. When strong northwest winds occur in summer, attention should be paid to forecasting EHT events.

Thanks for your listening!

Wang F., Wang Y., 2021. Potential role of local contributions to record-breaking high-temperature event in Xiamen, China. Weather and Climate Extremes. 33, 100338. https://doi.org/10.1016/j.wace.2021.100338.